EMI Suppression of High-Frequency Isolated Quasi Z-Source Inverter Based on Multi-Scroll Chaotic PWM Modulation

YAN CHEN[ID]1, WEIHAO JIANG1, YONG ZHENG2, AND GUODONGXU HE1
[1]School of Electrical and Electronic Engineering, Chongqing University of Technology, Chongqing 400054, China
[2]Engineering Research Center of Mechanical Testing Technology and Equipment, Ministry of Education, Chongqing University of Technology, Chongqing 400054, China

Corresponding author: Yong Zheng (sdzzzy@cqut.edu.cn)

ABSTRACT The high frequency isolated quasi Z-source inverter is a new type of inverter, which is suitable for photovoltaic generation system because of its high lift to voltage ratio, transient bridge direct access and electrical isolation.With the increase of its power density, the working frequency of its semiconductor switching devices is increasing. Switching devices in high-frequency states generate a large amount of electromagnetic noise, affecting the normal operation of surrounding electrical equipment and threatening the stability of the power grid. For the optimization of electromagnetic compatibility of high frequency isolation quasi Z-source inverter, using pulse width modulation (PWM) chaotic modulation technology, put forward using Chen multi-scroll chaotic system and traditional PWM are combined, using the new PWM control technology can inhibit electromagnetic interference (EMI) from the noise source, effectively reduce the high frequency isolation quasi Z-source switch frequency and its harmonics noise power, and optimize the total harmonic distortion (THD) of the output current by analyzing the chaotic modulation coefficient. Finally, the correctness of the theory is verified by Saber simulation and circuit test. This paper can provide guidelines for the electro magnetic compatibility (EMC) design of the high frequency isolated quasi Z-source inverter and provide the theoretical basis for the EMI optimization design of the power electronic system.

INDEX TERMS High frequency isolation quasi Z-source inverter, chaotic pulse width modulation (PWM) technology, multi-scroll chaos of Chen system, electromagnetic interference (EMI), total harmonic distortion (THD).

I. INTRODUCTION

Nowadays, diminishing fossil energy and environmental pollution stimulate the utilization of renewable energy, such as solar energy and wind energy. As a key component in these power generation systems, high-frequency switching device is widely used because of its small volume and high efficiency. However, the problem of serious electromagnetic interference (EMI) is frequently encountered to affect the safe operation of the entire power system due to the changes of high voltage and current in the switching device.

How to effectively suppress EMI is receiving more and more attention. In the literature, a improved operation

The associate editor coordinating the review of this manuscript and approving it for publication was Amedeo Andreotti[ID].

mode of high frequency switch has been proposed, which can reduce the peak of switching noise and improve the electromagnetic compatibility (EMC) of the switching circuit [1]–[3]. Different waveforms have been reported to spread the Pulse-Width Modulation (PWM) wave, including square wave [4], triangular wave [5] and sine wave [6]. However, the spectrums of these signals are not uniform, which cannot suppress the fixed frequency noise generated by the high-frequency switch. To remedy this defect, chaotic spread spectrum technology was invented, and then introduced to suppress EMI. The recent researches show that the chaotic spread spectrum technology could effectively reduce the peak value of the circuit noise by extending the switching frequency width [7]–[10]. Though better than a single waveform, the dynamical behavior of the chaotic signal generated

by Chua's circuit is relatively simple and its spectrum distribution is still not uniform enough for the fixed frequency noise [11].

In the past three decades, complex multiple volume wave chaotic systems have gradually become a research hotspot in nonlinear circuit theory [12]–[15]. A lot of chaotic systems have been proposed, including N- double volume wave is designed by Yalcin et al. [16], the circuit of 3, 5 volume wave is discovered by Yalcin et al. [17] and High order volume wave is realized by Lu and Cao [18], but these do not explain the effect of chaotic modulation on the output current ripple. Recently, the method of Multi-scroll Chaos in data encryption transmission has been successful. Ma et al. [19] proposed a kind of tensile Multi-scroll Chaos and applied it in secure communication. Zhang et al. [20] combines the self-regressive self-encoding random sequence with multi-rolling chaos to obtain a random sequence with high complexity and applies it to spread spectrum communication. For Hong Li, et.al, they use a 2*2-scroll chaotic attractor to suppress the peak of electromagnetic interference at the switch, thereby reducing the occurrence of low-order noise [21]. 2*2-scroll chaotic time domain waveform is simple and smooth, only suitable for simple circuit, can only suppress the generation of low-order noise, can not achieve good EMI suppression effect for complex high-order noise, 2*2-scroll chaotic can not EMI suppression of circuits under high frequency conditions. The signal of complex multi-scroll chaotic is more chaotic. It has abundant chaotic dynamic characteristics and multiple chaotic attractors. More importantly, its power spectrum is more average and continuous. Therefore, the Multi-scroll Chaos can further suppress the EMI of the circuit.

The high frequency isolated quasi Z-source inverter [22] has the characteristics of Z-source inverter, which allows direct access state. That is, the upper and lower bridge arms could be switched at the same time, but also has the characteristics of electrical isolation, high rise to voltage ratio, and low voltage and current stress. It is widely used in photovoltaic power generation systems. At present, the main research points for high frequency isolation quasi Z-source inverter are focused on topology improvement and practical engineering applications [23], [24], the research on the EMI analysis and suppression of the inverter is insufficient. In this paper, the EMI high frequency model of the inverter is set up and simulated by Saber. The experimental results show that the multi coil chaotic modulation can suppress the EMI of the circuit. Finally, the correctness of the theoretical analysis is verified by circuit experiments.

II. HIGH FREQUENCY ISOLATED QUASI Z-SOURCE INVERTER

A. HIGH FREQUENCY MODEL OF HIGH FREQUENCY ISOLATION QUASI Z-SOURCE INVERTER

Figure 1 gives the working principle diagram of high frequency isolation quasi Z-source inverter. When working in the zero-vector state, the switches $S_1 - S_4$ and S_5 are all turned on. In this state, the primary capacitor discharges,
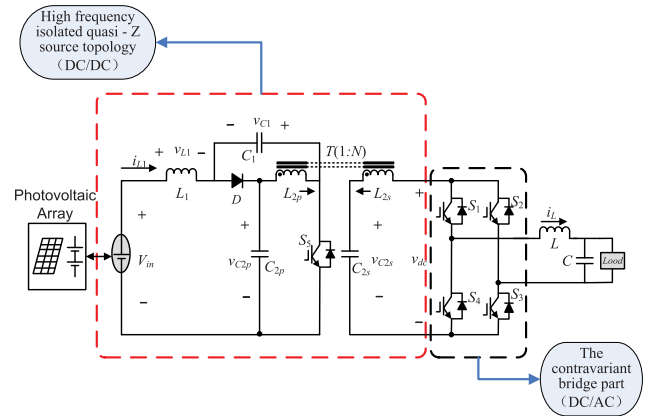

FIGURE 1. Principle diagram of high frequency isolated quasi Z-source inverter.

the inductor charges and the secondary capacitor charges, and the inverter bridge works in the freewheeling state without energy being transmitted. When working in the non-through state, the switch S_5 is open, the inverter works in an effective vector state, the primary capacitor is charged, the inductor discharges, the secondary capacitor discharges, and the energy is transmitted from the primary side of the transformer to the secondary side. Finally, transmit to load.

The ideal model of quasi Z-source inverter with high frequency isolation could not meet the needs of accurate simulation at high frequency. The parasitic parameters of the inverter have to be considered. For this inverter, the experiment needs to get the parasitics of all the passive components, power MOSFET, power diode, high frequency transformer and PCB circuit.

The network analyzer measures the resonant frequency of a passive component. The parasitic inductance of the capacitor could be calculated from Eq. (1), where Z is the capacitance impedance, R is the capacitance loss resistance, and L_{lead} is the lead inductance. Equation (2) could calculate the parasitic capacitance of the inductor, where Clead is the parasitic capacitance and L is the inductance.

$$Z = R + j(\omega L_{lead} - \frac{1}{\omega C}) \qquad (1)$$

$$C_{lead} = \frac{1}{\omega^2 L} \qquad (2)$$

Power MOSFET tubes and high-frequency transformers are the core components of the inverter,The power MOSFETs could be modeled using Model Architect in Saber, as shown in Fig. 2. R_d, R_g and R_s are drain resistance, gate resistance and source resistance respectively. The interelectrode capacitance (C_{ds}, C_{gd}, C_{gs}) can be obtained by consulting the chip technical manual.The model of the high-frequency transformer is shown in Fig. 3, R_p, R_s is the winding resistance, L_{p-leak} and L_{s-leak} are the leakage inductance of the winding, C_p, C_s are the distributed capacitance of the winding, C_{ps} is the winding capacity of the primary and secondary windings. The original secondary winding resistance and the original
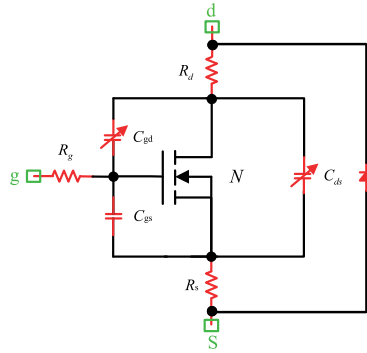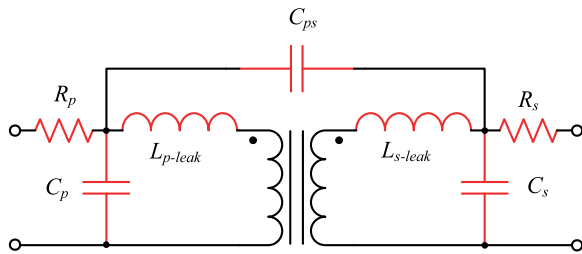
FIGURE 2. High frequency model of power MOSFET.
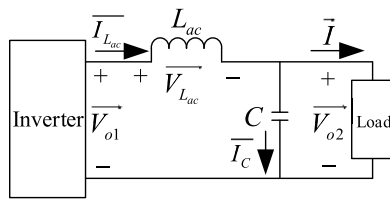

FIGURE 3. High frequency model of transformer.

FIGURE 4. Equivalent circuit diagram of high frequency isolated quasi Z-source inverter.

TABLE 1. High frequency parameters of high frequency isolated quasi Z-source inverter.

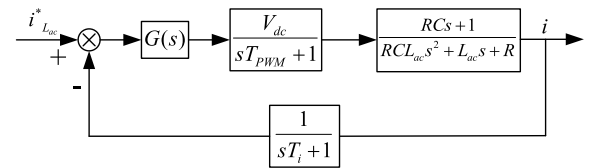| High-frequency parameters	Numerical value
Primary inductance parasitic capacitance C_{lead}/pF	75.6
Primary inductance loss resistor R/Ω	0.06
Primary side capacitor parasitic inductance L_{lead}/nH	45.6
Primary capacitance loss resistor R/Ω	0.17
Secondary side parasitic inductance L_{lead}/nH	78.3
Secondary capacitor loss resistor R/Ω	0.22
Transformer primary winding resistance R_p/Ω	0.12
Transformer secondary winding resistance R_s/Ω	0.23
Transformer primary winding leakage inductance $L_{p-leak}/\mu H$	13.2
Transformer secondary winding leakage inductance $L_{s-leak}/\mu H$	48.7
Transformer primary winding distributed capacitance C_p/pF	64.7
Transformer secondary winding distribution capacitance C_s/pF	114.6

FIGURE 5. Block diagram of the current control loop.

secondary winding capacitance could be measured directly by the LCR tester, the winding leakage inductance could be measured by the short circuit method, the primary distribution capacitance could be calculated using the network analyzer to measure the primary impedance characteristics get the resonant frequency.

High-frequency parameters of high-frequency quasi quasi Z-source inverter could be obtained through the test and calculation, the inverter's main components parameters are shown in Table 1.

B. CONTROL STRATEGY OF HIGH FREQUENCY ISOLATION QUASI Z-SOURCE INVERTER

The difference between the output voltage of the inverter and the load voltage generates the inductor current in the filter circuit, as shown in Fig. 4. In the figure, $\overrightarrow{V_{o1}}$ is the output voltage of the high frequency isolated quasi Z-source inverter. $\overrightarrow{I_{Lac}}$ is the current of the filter inductor L_{ac}, and $\overrightarrow{I_C}$ is the current of the filter capacitor C. The voltage of the filter inductor L_{ac} is $\overrightarrow{V_{Lac}}$, $\overrightarrow{I}$ is the load current, and $\overrightarrow{V_{o2}}$ is the load voltage.

The transfer function of the inductor current can be obtained by analyzing and performing the Laplace transform:

$$i_{Lac} = \frac{MV_{dc}(RCs+1)}{RCL_{ac}s^2 + L_{ac}s + R} \tag{3}$$

According to the above analysis, a block diagram of the current control loop can be obtained as shown in Fig. 5. In the figure, $G(s)$ is the controller of the current control loop; T_i is the load current sampling inertia time constant; T_{PWM} is the modulation switching period.

According to the above analysis, the current controller $G(s)$ adopts a quasi-PR regulator to achieve high gain in a small range around the fundamental frequency, so that the system can work normally even in the case of a small range of frequency offset. The transfer function of the quasi-PR regulator is:

$$G_{PR}(s) = K_P + \frac{2K_R\omega_c s}{s^2 + 2\omega_c s + \omega_0^2} \tag{4}$$

In the formula, ω_o is the power frequency angular frequency, corresponding to the power frequency $50Hz$,

$\omega_o = 314 rad/s$. The loop gain of the system is derived by deriving:

$$G_i(s) = \frac{G_{PR}(s)V_{dc}(RCs + 1)}{(RCL_{ac}s^2 + L_{ac}s + R)(sT_{PWM} + 1)(sT_i + 1)} \quad (5)$$

Substituting Eq. 4 into Eq. 5 can be obtained:

$$G_i(s) = \frac{[K_P(s^2 + 2\omega_c s + \omega_0^2) + 2K_R\omega_c s]V_{dc}(RCs + 1)}{(RCL_{ac}s^2 + Ls + R)(sT_{PWM} + 1)} \\ (sT_i + 1)(s^2 + 2\omega_c s + \omega_0^2) \quad (6)$$

It can be seen from the above formula that the quasi-PR regulator has three parameters to be designed, K_P, K_R, ω_c. These three parameters are closely related to system performance, and then the three parameters are optimized. In this study, the control variable method is used to align the three parameters of the PR regulator, that is, the two parameters are kept unchanged, and the influence of the third parameter change on the system performance is investigated.

First, we will examine the influence of the parameter ω_c change on the system, keep $K_P = 0$, $K_R = 1$ unchanged. According to the analysis, as the ω_c increases, the bandwidth and gain of the controller increase, and the corresponding harmonic amount also increases. Therefore, ω_c must be determined based on the actual required bandwidth. The bandwidth is the difference between the two frequencies at the gain drop of 3dB on the amplitude-frequency response curve, so we can get:

$$|G_{PR}(j\omega)| = \left| \frac{2\omega_c(j\omega)}{(j\omega)^2 + 2\omega_c(j\omega) + \omega_0^2} \right| \\ = \left| \frac{1}{1 + \frac{j(\omega^2 + \omega_0^2)}{2\omega_c\omega}} \right| = \frac{1}{\sqrt{2}} \quad (7)$$

Solving Eq. 7 gives the bandwidth of the quasi-PR regulator at this time:

$$BW = \frac{\omega_c}{\pi} Hz \quad (8)$$

In order to satisfy the voltage frequency fluctuation range of $\pm 0.5 Hz$, the corresponding bandwidth is $1 Hz$, thereby obtaining $\omega_c = \pi rad/s$.

Consider the influence of the parameter K_R change on the system, keep $K_p = 0$, $\omega_c = \pi rad/s$ unchanged. According to the analysis, as the K_R increases, the phase-frequency characteristic curve of the system does not change, the bandwidth does not change, and the system gain gradually increases. An increase in system gain will cause the load current steady-state error to decrease. Therefore, a compromise of $K_R = 18$ ensures that the system has sufficient gain near the fundamental frequency.

Finally, we examine the influence of the parameter K_P change on the system, keep $K_R = 18$, $\omega_c = \pi rad/s$ unchanged. According to the analysis, as the K_P increases,
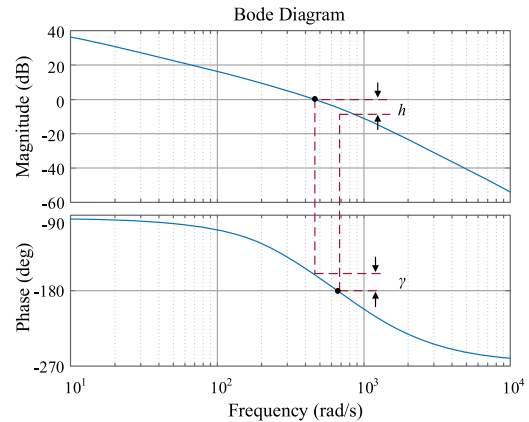

FIGURE 6. Current control loop open-loop transfer function frequency response diagram.

the gain of the system gradually increases, and the anti-interference ability is enhanced, but the stability of the system is lowered. Therefore, the compromise chooses $K_P = 0.2$.

In summary, the final parameters of the design of the quasi-PR regulator are: $K_P = 0.2$, $K_R = 18$, $\omega_c = \pi rad/s$. Therefore, the transfer function of the quasi-PR regulator is:

$$G_{PR}(s) = 0.2 + \frac{36\pi s}{s^2 + 2\pi s + (100\pi)^2} \quad (9)$$

Combining the above-mentioned parameters into the block diagram of the load current control loop, Fig. 5 shows the open loop transfer function of the current control loop:

$$W_O(s) = \frac{G_{PR}(s)V_{dc}(RCs + 1)}{(sT_{PWM} + 1)(RCL_{ac}s^2 + Ls + R)(sT_i + 1)} \quad (10)$$

The frequency response diagram of the open-loop transfer function of the current control loop is made using MathCAD, as shown in Fig. 6.

In the case of selecting the above-mentioned quasi-PR regulator parameters, we can see that the stability margin of the current control loop system can be reflected from the phase margin of the gain margin indicated in the Fig. 6. In order to stabilize the system, according to the Nyquist criterion, the phase margin γ of the open-loop transfer function must be greater than zero, and the gain margin h must be greater than 3dB. According to Fig. 6, $h > 3dB$ and $\gamma > 0$, which shows that the designed system in this paper is stable.

III. MULTI-SCROLL CHAOS BASED ON CHEN SYSTEM

Chua's chaotic circuit is the most basic chaotic circuit. It has a simple structure and good chaotic dynamics. The composition of the Chua's circuit is shown in Fig. 7, where R, L, C_1 and C_2 form the main body of the Chua's chaotic circuit. The amplifiers T_1 and T_2 and the resistors R_1 to R_6 in the block form a nonlinear resistor R_N. By adjusting the size of the resistors $R_1 - R_6$, the operating areas of the two amplifiers are reversed. The amplifier T_1 operates in the linear region and the amplifier T_1 operates in the saturation region to achieve nonlinear resistance characteristics. The nonlinear resistance
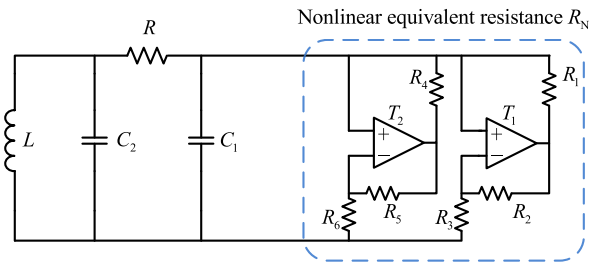
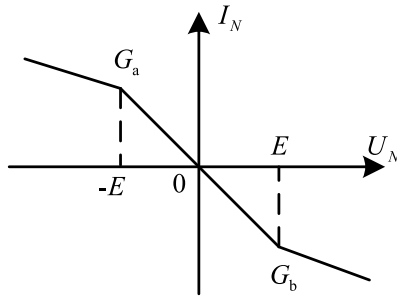**FIGURE 7. Chua's chaotic circuit diagram.**

FIGURE 8. Resistance R_N characteristic curve.

characteristics shown in Fig. 8 can be realized, where G_a and G_b are the slopes of the internal and external volt-ampere characteristics of the nonlinear resistance, respectively, and E is the turning point voltage. By simulation, when $R_1 = R_2 = 220\Omega$, $R_4 = R_5 = 22k\Omega$, $R_2 = 2.2k\Omega$, $R_6 = 3.3k\Omega$, $C_1 = 10nF$, $C_2 = 100nF$, $L = 18mH$, $R = 1.57k\Omega$, the circuit generates a stable chaotic signal.

Let $x = U_1/E$, $y = U_2/E$, $z = Ri_L/E$, $a = RG_a$, $b = RG_b$, $\alpha = C_2/C_1$, $\beta = R^2C_2/L$. Where U_1 and U_2 are the voltages of capacitors C_1 and C_2, i_L is the current flowing through inductor L, and $f(U_1)$ is a function of nonlinear resistor R_N. Then the equation of state can become:

$$\begin{cases} \dot{x} = \alpha (y - x - f(x)) \\ \dot{y} = x - y + z \\ \dot{z} = -\beta y \\ f(x) = bx + \frac{1}{2}(a - b)(|x + 1| - |x - 1|) \end{cases} \quad (11)$$

Multi-scroll chaos is a research hotspot at present. Many researches have been done in the field of data encryption and transmission. Some rasearch in EMI suppression of switching power supply has rarely been reported now [25]–[28]. In this study, a multi-scroll chaotic modulation technology is proposed to suppress the EMI of switching power supply. Based on piecewise Chen system, a multi segment linear function is constructed as a switcher and a new chaotic attractor is generated in this system. The expression of the state equation of the Chen system is as follows:

$$\begin{cases} \dot{x} = -ax + ay \\ \dot{y} = (b - z)sgn(x) + cy \\ \dot{z} = xsgn(y) - dz \end{cases} \quad (12)$$

Replacing the Eq. (12) into a new even symmetric piecewise linear function $f_c(y)$, It can be expressed in the

following form:

$$f_c(y) = |ky| + \sum_{n=1}^{N} C_n \begin{bmatrix} step(y + E_n) \\ +step(-y - E_n) \end{bmatrix} \quad (13)$$

Among them, $sgn(x)$ is Symbolic function of x, $step(y) = sgn(y) + 1$, N is the order of controlling chaos. Volume of coiling waves is $2N + 2$, C_n is to control the output amplitude of chaotic signals at different stages, E_n is the level of chaotic signal level at different stages.The values of the E_n and C_n can be limited by the Eq. (14):

$$\begin{cases} E_n = \dfrac{nE_{max}}{k} \\ C_n = \dfrac{k(E_n - E_{n-1})}{2} - \varepsilon \end{cases} \quad (14)$$

Let $\dot{x} = \dot{y} = \dot{z} = 0$, Simultaneous Eqs. (12) and (13) can be obtained:

$$\begin{cases} x_{\pm n} = y_{\pm n} \\ z_{\pm n} = b + \dfrac{cy_{\pm n}}{sgn(x_{\pm n})} \\ f_c(y_{\pm n}) = bd + \dfrac{cdy_{\pm n}}{sgn(x_{\pm n})} \end{cases} \quad (15)$$

The equilibrium point can be obtained by solving the above equation:

$$\begin{cases} x_{\pm n} = \pm\dfrac{bd + 2\sum_{i=0}^{n} C_i}{k - cd} \\ y_{\pm n} = \pm\dfrac{bd + 2\sum_{i=0}^{n} C_i}{k - cd} \\ z_{\pm n} = \pm\dfrac{bcd + 2c\sum_{i=0}^{n} C_i}{k - cd} + b \end{cases} \quad (16)$$

If $a = 1.18$, $b = 5.82$, $c = 0.7$, $k = 4$, $N = 3$, $\varepsilon = 0.16$, $E_{max} = 2$, $C_0 = 0$.The solution (16) gets the equilibrium point as follows:

$$\begin{cases} Q \pm 0(\pm0.2518, \pm0.2518, 5.9963) \\ Q \pm 1(\pm0.6640, \pm0.6640, 6.2848) \\ Q \pm 2(\pm1.1323, \pm1.1323, 6.6126) \\ Q \pm 3(\pm1.6006, \pm1.6006, 6.9404) \\ Q \pm 4(\pm2.0689, \pm2.0689, 7.2682) \end{cases} \quad (17)$$

The equation of the middle equilibrium point in the corresponding upper formula is obtained by

the Eqs. (12) and (13).

$$
\begin{cases}
\pm Q_0 : \begin{cases} \pm\alpha_0 = -1.180 \\ \beta_0 \pm j\gamma_0 = 0.266 \pm j1.952 \end{cases} \\
\pm Q1 : \begin{cases} \pm\alpha_1 = -1.180 \\ \beta_1 \pm j\gamma_1 = 0.266 \pm j1.952 \end{cases} \\
\pm Q2 : \begin{cases} \pm\alpha_2 = -1.180 \\ \beta_2 \pm j\gamma_2 = 0.266 \pm j1.952 \end{cases} \\
\pm Q3 : \begin{cases} \pm\alpha_3 = -1.180 \\ \beta_3 \pm j\gamma_3 = 0.266 \pm j1.952 \end{cases} \\
\pm Q4 : \begin{cases} \pm\alpha_4 = -1.180 \\ \beta_4 \pm j\gamma_4 = 0.266 \pm j1.952 \end{cases}
\end{cases} \tag{18}
$$

From the upper form $\pm Q_0, \pm Q_1, \pm Q_2, \pm Q_3, \pm Q_4$ are the equilibrium point. Therefore, 10 wave chaotic attractors can be generated.

IV. FREQUENCY MODULATION BASED ON CHAOTIC SIGNAL

The theoretical basis of spread spectrum technology is Parseval's theorem. If the sum of the energy in the time domain of the signal remains the same, the sum of the energy in the frequency domain also remains the same. Therefore, by extending the switching frequency, the band width near the switching harmonic frequency could be increased and the peak value of the switching harmonic could be reduced. In this paper, spread spectrum technology adopts chaotic frequency signal to replace fixed switching frequency, so as to expand frequency band width and reduce EMI effect. Usually, the waveform of a switching converter is not a sine wave in nature, but contains a myriad of switching harmonics. The frequency modulation of the PWM pulse is to redistribute the spectrum of each switching harmonic to the sideband harmonics of the switching harmonics. Moreover, the frequency difference between every two adjacent sideband harmonics is still f_m. The Carson rule can still be used to calculate the bandwidth of the nth switching harmonic, as in Eq. (19).

$$
\beta_{nT} = 2(\beta_n + 1)f_m = 2(n\beta + 1)f_m \tag{19}
$$

In the formula, β_n is the nth switching harmonic modulation coefficient, $\beta_n = n\beta$. When $\beta \gg 1$, $\beta_{nT} = n\beta_T$. It can be concluded from Eq. (19) that as the harmonic order of the switch increases, the effect of spectrum unwrapping increases, and finally, on the higher switching harmonics, the sideband harmonics of adjacent switching harmonics overlap each other. That is to say, as the harmonic order of the switch increases, the spectrum spread is more uniform. Therefore, when the signal of the continuous spectrum is used as the modulated baseband signal, the spectrum of the signal can be more uniform and a better spread spectrum effect can be achieved. Therefore, it can be foreseen that the chaotic carrier frequency PWM modulation scheme can reduce the switching noise more effectively than the conventional PWM modulation scheme. Schematic diagram of the principle of chaotic spread spectrum method is shown as in Fig. 9.

For multi-scroll chaotic PWM modulation, the spread spectrum frequency Δf is generated by multi-scroll chaotic
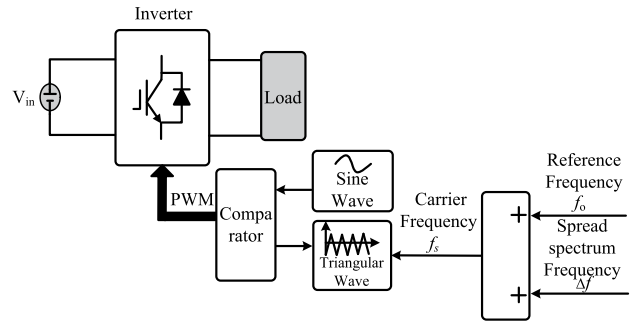

FIGURE 9. Schematic diagram of the principle of chaotic spread spectrum method.
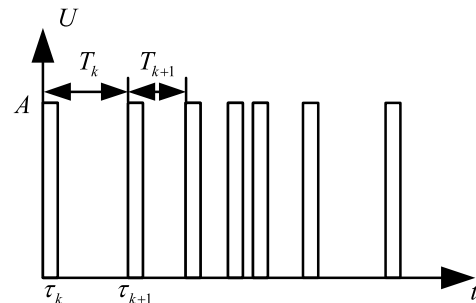

FIGURE 10. Chaotic frequency PWM waveform.

attractors. Firstly, multi-scroll wave attractors are generated according to the multi-scroll chaotic system state equation, and then the state in the chaotic attractor. The variables are sampled to obtain a series of chaotic sequences in chaotic state. The carrier signal f_s with frequency chaos change is compared with the modulated wave to generate chaotic pwm control signal, and the switching of the switching device of the power electronic converter is controlled, thereby realizing multi-scroll chaotic PWM control of the power electronic converter.

In the system shown in Fig. 9, the maximum amplitude of the harmonic voltage of the output line voltage appears at the triangular carrier frequency f_s, and the harmonic voltage is $U_h(t)$.

$$
U_h(t) = U_h \sin 2\pi f_s t = U_h \sin 2\pi (f_0 + \Delta f)t \tag{20}
$$

The frequency of the switching converter PWM after chaotic spread spectrum can be expressed as:

$$
f(t) = f_0 + \Delta f = k_1 v + k_2 \Delta v \tag{21}
$$

Among them f_0 is the base frequency of the switch, Δf the chaotic frequency of the switch, v is the basic voltage to determine the switching frequency, Δv is the chaotic voltage determining the chaotic frequency of the switch, k_1 and k_2 are the amplification coefficients of the basic voltage and the chaotic voltage, respectively. Obviously, according to Eq. (21), when Δf is zero, is the normal fixed-frequency PWM modulation; When Δf chaos changes, it is PWM of chaotic spread spectrum, and the waveform is shown in Fig. 10.
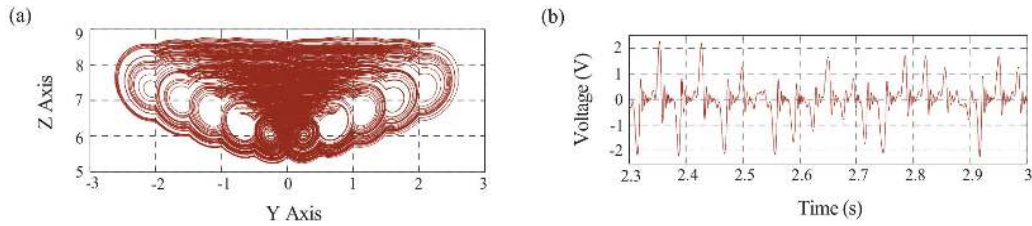
FIGURE 11. 10 scroll chaotic graph: (a) 10 volume wave chaotic attractor; (b) 10 volume wave chaotic time domain diagram.

According to the PWM control principle of the power electronic converter, the modulated wave signal is compared with the carrier signal to generate the control signal of the switching device. In the variable frequency chaotic PWM control, the PWM signal is generated by comparing the modulated signal with the carrier signal of the frequency chaotic change, and the power electronic conversion is controlled. The device works to realize the implementation of chaotic PWM.

A is the amplitude of the pulse voltage, T_k is the interval between k pulses and $k + 1$ pulses. τ_k is the starting time of k pulse. From Figure 10, the period of chaotic PWM is changed, the change rule of T_k is determined by Δf. The chaotic changes in the set of T_k can be described by the function ξ:

$$T_k = \xi(T_{k-1}) \tag{22}$$

Then τ_k can be expressed as:

$$\tau_k = T_1 + T_2 + \cdots T_{k-1}$$
$$= T_1 + \xi(T_1) + \cdots \xi^{k-1}(T_1) \tag{23}$$

In this paper, the chaotic PWM waveform is regarded as a discrete pulse and is represented by $\delta(t)$. Then the Fourier transform can be expressed as:

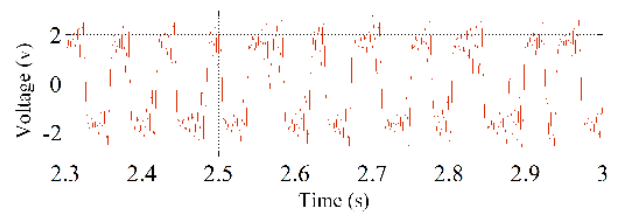$$\delta_T(j\omega) = \sum_{i=1}^{M_t} A e^{-j\omega\tau_i} \tag{24}$$

In the form of T at a certain moment, M_t is the number of all pulses before the moment T. The power $\delta(t)$ spectrum function of the chaotic PWM pulse is as follows:

$$S(\omega) = \lim_{T \to \infty} \frac{1}{T} E(|\delta_T(j\omega)|^2) \tag{25}$$

The Eq. (27) substitution Eq. (28) can be obtained:

$$|\delta_T(j\omega)|^2 = \left| \sum_{i=1}^{M_{t1}} \sum_{j=1}^{M_{t2}} A e^{-j\omega\tau_i} A e^{-j\omega\tau_j} \right| \tag{26}$$

$$|\delta_T(j\omega)|^2 = \sum_{i=1}^{M_{t1}} A^2$$
$$+ 2 \sum_{i=1}^{M_{t1}-1} \sum_{j=1}^{M_{t2}-i} A^2 \cos\left[\omega\left(\tau_{i+j} - \tau_i\right)\right] \tag{27}$$

FIGURE 12. Chua's chaotic time domain waveform.

$$S(\omega) \approx \frac{1}{E(T_k)} A^2 + 2 \lim_{T \to \infty} \frac{1}{E(T_k)} A^2$$
$$\times \sum_{i=1}^{M_{t1}-1} \sum_{j=1}^{M_{t2}-i} E \cos\left[\omega\left(\tau_{i+j} - \tau_i\right)\right] \tag{28}$$

Because τ_k is irregular in chaotic PWM pulse sequence Eq. (27) and $\omega(\tau_{i+j} - \tau_i)$ is continuous and distributed on a certain bandwidth on the spectrum, so the noise power will be dispersed in a certain frequency band instead of aggregating at fixed frequency.

V. SIMULATION OF EMI SUPPRESSION SIMULATION OF HIGH FREQUENCY ISOLATED QUASI Z-SOURCE INVERTER
A. SIMULATION ANALYSIS OF MULTI-SCROLL CHAOTIC
The multi-scroll chaotic system has more key parameters. Most of the chaotic attractors are distributed in multiple directions in the phase space, and the wavelets have nested topologies. In terms of dynamic characteristics, multi-scroll chaotic systems have more complex dynamic characteristics. The phase trajectory or state variable of a chaotic attractor jumps between several different chaotic attractors. The multi volume wave chaotic circuit is built by saber, and the order volume wave chaos could be generated by changing the value in the Eq. (13). In the circuit design, the multi-scroll chaotic could be realized by setting a limited level step. When the value is 4, the 10 volume wave chaos, as shown in Fig. 11, is obtained, in which (a) is a 10 volume wave chaotic attractor, and (b) is a 10 volume wave chaotic spectrum.

Through the derivation of mathematical expressions and dynamics analysis, the chaotic attractor of the 10-volume Chen system is realized. The voltage waveforms of x, y,
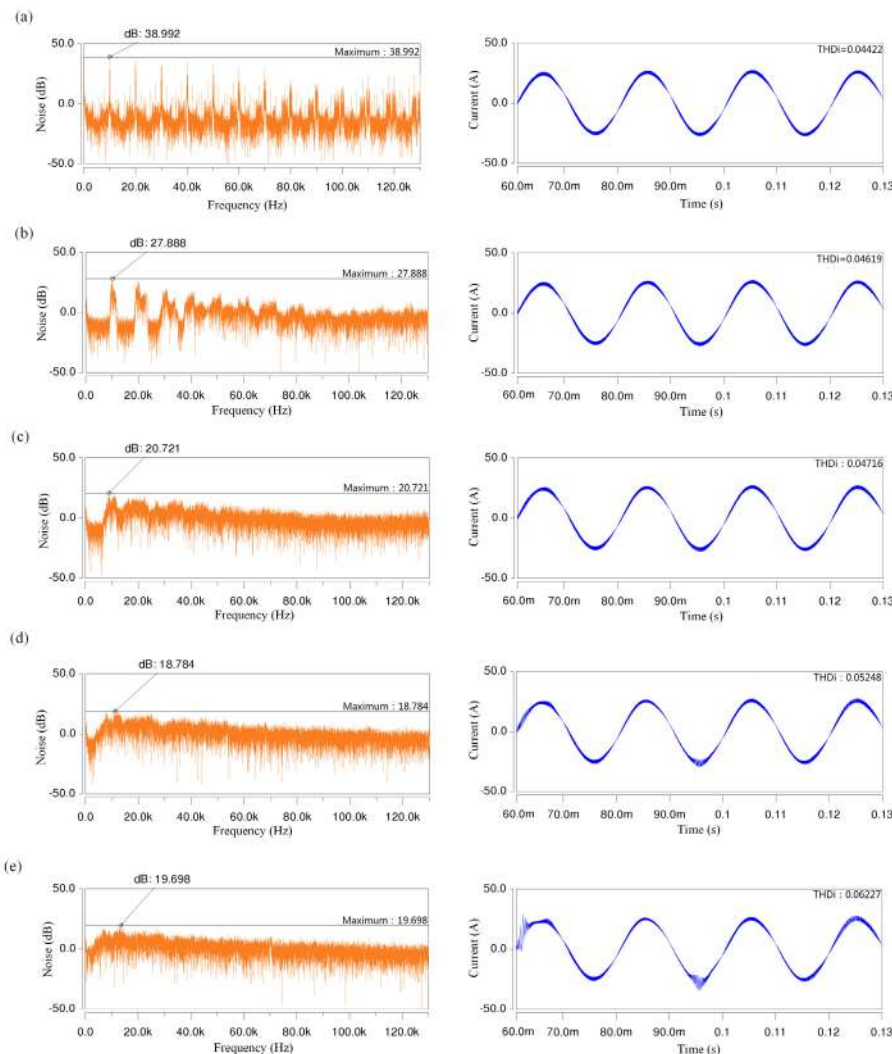
FIGURE 13. Circuit noise and output waveform under different spread spectrum depth:(a) EMI and output waveform in conventional mode; (b) Circuit EMI and output waveform of 10 volume wave chaotic under 1% spreading factor; (c) Circuit EMI and output waveform of 10 volume wave chaotic under 5% spreading factor; (d) Circuit EMI and output waveform of 10 volume wave chaotic under 10% spreading factor; (e) Circuit EMI and output waveform of 10 volume wave chaotic under 15% spreading factor.

and z can be obtained by Simulink simulation. In the circuit experiment, the voltage waveform and chaotic phase diagram can be obtained by RT-LAB hardware-in-the-loop simulation, which realizes the multi-wing shape of the multi-scroll chaos in Chen system, and can clearly see the 10 attractors of the multi-scroll chaos in Chen system. Fig. 12 shows the voltage waveform of Chua's chaos.

It can be seen from the Fig. 12 that the time domain waveform of Chua's chaos has no fixed period and the amplitude changes randomly. Chua's chaos can provide a stable and reliable chaotic spread spectrum signal for chaotic spread spectrum modulation. However, compared with multi-scroll chaos, the time domain waveform is shown in Fig. 11(b), the same time period, the Chua's chaotic time domain waveform is relatively simple and simple, and the variability

is small, while the multi-scroll chaotic time domain waveform is complex and disordered, and the variability is large. By observing the image, it can be seen that the time domain waveform of the multi-scroll chaos in the Chen system is more disordered and has more complex dynamic behavior characteristics. Chen system multi-scroll chaos x time domain waveform step more, the waveform change is more complicated in the same period of time, its complexity is applied to the high frequency isolated quasi Z-source inverter, EMI suppression effect is better. Spreading the modulation using the chaos increases the chaotic variation of the PWM period, which is beneficial to the uniform distribution of the conducted noise over a certain width spectrum. Therefore, this paper will use multi-scroll chaos for spread spectrum modulation to suppress circuit EMI and analyze the stability of the system.
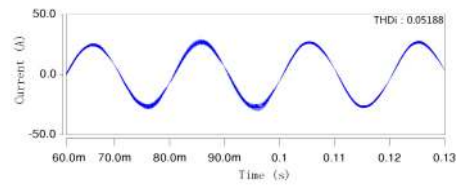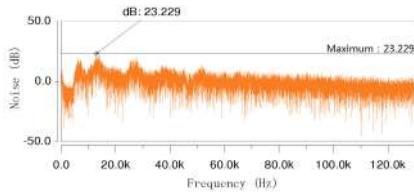
FIGURE 14. Circuit noise and output waveform of Chua's chaotic spread spectrum 5%.
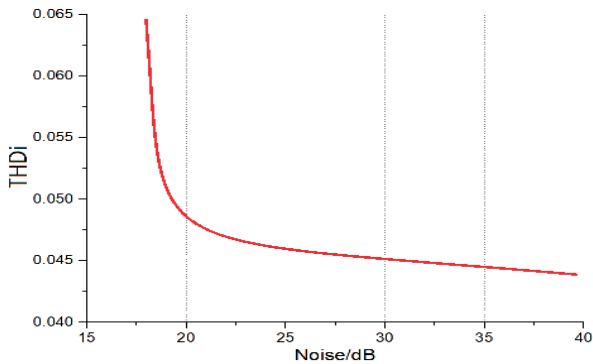

FIGURE 15. Relationship between circuit noise and THD with different spread spectrum modulation coefficients.

FIGURE 16. Circuit experiment.

B. SIMULATION ANALYSIS OF EMI SUPPRESSION FOR HIGH FREQUENCY ISOLATED QUASI Z SOURCE INVERTER

In this paper, a high frequency model of high frequency isolated quasi Z-source inverter is established in Saber. EMI suppression is carried out by using multi-scroll chaotic spread spectrum. Through simulation, the transmission noise spectrum and output current waveform THD under different spread spectrum parameters could be obtained. Firstly, EMI simulation is performed on the high frequency isolated quasi Z-source inverter under conventional PWM modulation, and then EMI suppression simulation is performed using multi-scroll chaos with different spreading factors. Finally, the EMI suppression simulation of Chua's chaos under the same spreading factor as multi-scroll chaos is used to prove the superiority of multi-scroll chaos suppression EMI. As shown in Fig. 13.(a), this is the EMI spectrum and circuit output THD when the multi-scroll chaotic spread spectrum is not used in the conventional mode. The noise is concentrated at 10kHz and its multiples, and spikes are generated in these places. The maximum noise is 38.992dB at 10kHz. And the THD of the output waveform is higher, and the THD is 0.04422. As shown in Fig. 13. (b), (c), (d), (e) are the conduction noises and output waveforms of the inverter when the chaotic spread spectrum modulation coefficients are 1%, 5%, 10% and 15% respectively. It can be seen from the simulation results that the EMI peak can be greatly reduced by using a small spreading factor. Using 10 volume wave chaotic can reduce the EMI peak from 38.992dB to 27.888dB, 20.721dB, 18.784dB, 19.698dB. The EMI suppression effect has been greatly improved. Compared with Fig. 14, under the
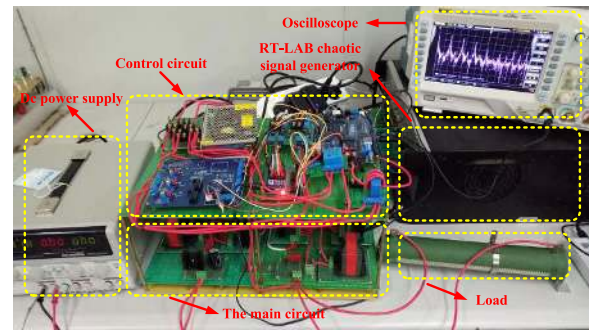
same 5% spreading factor, 10 volume wave chaotic is better than the Chua's chaotic EMI suppression. However, with the increase of the spreading factor, the circuit THD has a slight influence. The Multi-scroll Chaos which has less affection in output power quality and more uniform spectrum could have better effect in the suppression of EMI in spread spectrum than the based Chua's chaos.

In this paper, the relationship between the amplitude of noise and the ripple of output voltage is obtained through a lot of simulation, and the curve shown in Fig. 15 could be obtained by fitting. When the modulation coefficient of chaotic spread spectrum is at $5\% - 10\%$, the circuit noise is smaller and the circuit ripple is smaller. When the value is 6.3%, the noise is 19.701dBV and THD is 0.04723.

VI. EXPERIMENTAL VERIFICATION

To verify the above theoretical analysis and the correctness of inverter circuit simulation, relevant circuit verification analysis is carried out, and a high frequency isolation quasi Z-source inverter circuit model based on proportional control mode is built. Fig. 16 shows a Circuit diagram for conducting EMI test. The high frequency isolated quasi Z-source inverter model is divided into upper and lower layers. The upper layer is mainly equipped with power switch tube drive circuit, sampling circuit, DSP controller and other modules. The lower layer is the high frequency isolated quasi Z-source inverter main circuit, including the boost section and the inverter section. The multi-scroll chaotic circuit is provided by the RT-LAB simulator, and the drive circuit uses the 6N137 drive chip. Circuit parameters: input voltage $V_{in} = 32V$, $f = 20kHz$, load resistance $R = 10\Omega$, filter inductance of high frequency isolated quasi Z-source inverter $L = 8mH$, filter capacitor $C = 20\mu F$, isolation transformer ratio $N = 2$.
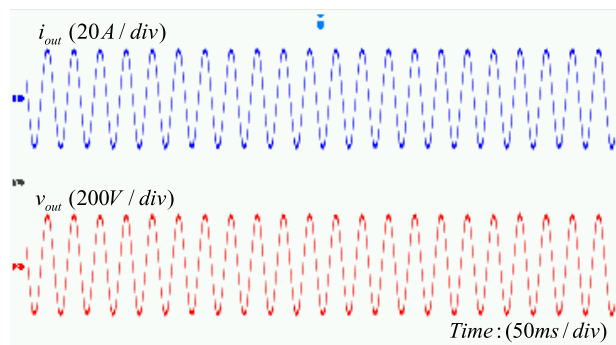
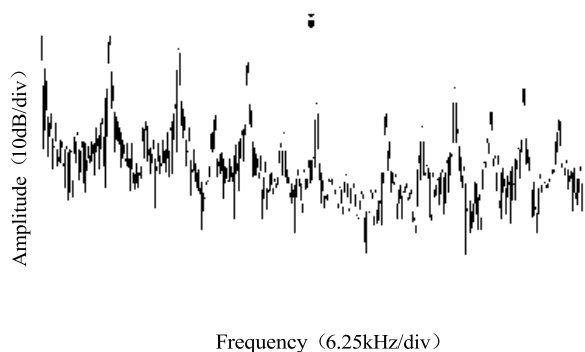**FIGURE 17.** Circuit output current and voltage waveform.

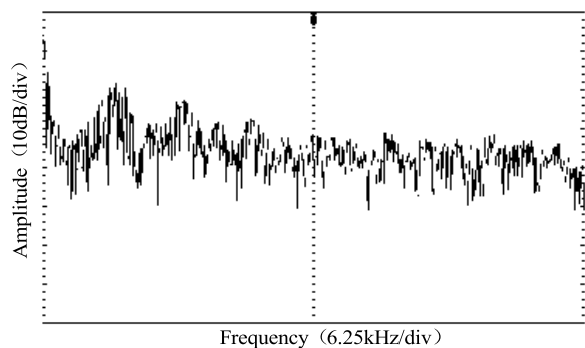**FIGURE 18.** Circuit experiment noise spectrum in normal mode.

FIGURE 19. Experimental noise spectrum of circuit in multi-scroll chaotic PWM modulation mode.

In this paper, the current control loop quasi-PR regulator is used. The output current and voltage waveform of the high frequency isolated quasi Z-source inverter load terminal are shown in Fig. 17. As can be seen from the waveforms in the figure, the output current is stable at 22A, the output voltage is stable at 220V, and the theoretical ideal value is reached.

The frequency spectrum of the circuit is measured as shown in Fig. 18. The noise spectrum of the multi-scroll chaotic spread spectrum with modulation coefficient of 6.3% is measured as shown in Fig. 19.

Based on the experimental results, we can conclude that after the suppression of EMI by the multi-scroll chaotic

spread spectrum, the circuit noise has been greatly improved, and 19.3dB has been reduced at the switching frequency.

VII. CONCLUSION

The paper mainly studies the electromagnetic isolation of high-frequency quasi Z-source inverter under the proportional control. By modelling the components of the inverter and analyzing the circuit noise under different chaotic spread spectrum modulation coefficients and the corresponding output current THD, describing the relationship between suppression of EMI capability and corresponding THD for inverters that use the multi-scroll chaotic theory. When the modulation coefficient is 6.3%, THDi value and EMI suppression effect are optimal. With the same modulation system, Chen system 10 wave chaos has better EMI suppression effect than Chua's chaos and has less impact on the output power quality. Multi-scroll chaotic with more uniform spectrum has better EMI suppression effect than basic Chua's chaos. The results confirm the correctness of the theoretical analysis using the circuit model and simulation, which is also verified by the experimental date. This paper could provide a reference for the design of electromagnetic compatibility of high frequency isolated quasi Z-source inverter, and also provide a theoretical basis for EMI optimization design of power electronic system.

REFERENCES

[1] Q. Sun, K. X. Wei, S. S. Wang, L. Bin, and C. Gao, "Mechanism study on wideband modeling of transmission lines considering distributed parameters for PWM converters," *Chin. Soc. Elect. Eng.*, vol. 36, no. 15, pp. 4232–4241, 2016.

[2] Z. H. Ma, J. F. Xia, B. C. Bao, and J. Sha, "Dual pulse skipping modulation technique for buck converter operating in discontinuous conduction mode," *Chin. Soc. Elect. Eng.*, vol. 33, no. 12, pp. 24–31, 2013.

[3] Y.-D. Liu, H. Li, B. Zhang, Q. L. Zheng, and X.-J. You, "Spectrum calculation of chaotic SPWM signals based on double Fourier series," *Acta Phys. Sinica*, vol. 63, no. 7, 2014, Art. no. 70503.

[4] B. Qian, Y. X. Feng, and S. C. Pan, "TDDM-BOC modulation signal parameter estimation method," *Inf. Control*, vol. 134, pp. A635–A646, Dec. 1965.

[5] C. Qi, X. Y. Chen, and X. M. Mu, "A hybrid spread spectrum modulation technique for PWM inverters," *Chin. Soc. Elect. Eng.*, vol. 32, no. 24, pp. 38–44, Aug. 2012.

[6] C. Wang and H. L. Zhang, "Parameter identification for fractional-order multi-scroll chaotic systems based on original dual-state transition algorithm," *Acta Phys. Sinica*, vol. 65, no. 6, pp. 52–60, Mar. 2016.

[7] J. Yan, J. Wang, Y. Xu, P. Wang, K. Huang, and P. Hou, "Influence of neutral-point voltage deviation of PWM converter on insulation monitoring in medium-voltage networks," *IEEE Trans. Power Del.*, vol. 32, no. 4, pp. 1730–1738, Aug. 2017.

[8] R. Yang, B. Zhang, and D. Y. Qiu, "Qiu Chaotic point process description of converter discrete subsystem and EMI suppression," *Acta Phys. Sinica*, vol. 57, no. 3, pp. 1389–1397, 2008.

[9] P. Wang, F. Zheng, X. Yang, and G. Peng, "A method for adjusting common mode noise impedance and optimizing EMI filters," *Chin. Soc. Elect. Eng.*, vol. 34, no. 6, pp. 993–1000, 2014.

[10] J. Y. Niu, Z. Li, and Y. H. Song, "Application of chaotic carrier-frequency modulation in commercial switch mode power supply," *Power Supply Technol. Its Appl.*, vol. 40, no. 8, pp. 65–71, 2014.

[11] G. Q. Zhong, "Chuas circuit chaotic synchronization secure communication," *J. Circuits Syst.*, pp. 19–29, 1996.

[12] K. H. Sun, X. X. Ai, and S. B. He, "Design of multi-scroll hyperchaotic system and analysis on its characteristic," *J. Cent. South Univ. (Sci. Technol.)*, no. 5, pp. 1663–1672, May 2015.

[13] X. J. Li and D. H. Zhou, "A method of chaotic secure communication based on strong tracking filter," *Acta Phys. Sinica*, vol. 64, no. 14, pp. 65–71, Jul. 2015.

[14] L. X. Wang, Y. Q. Wang, Z. P. Chen, and M. Zhang, "Research on anti-jamming performance of spread spectrum communication system based on simulink," *Microcomput. Appl.*, vol. 35, no. 22, pp. 68–71, 2016.

[15] E. Tlelo-Cuautle, A. D. Pano-Azucena, J. J. Rangel-Magdaleno, V. H. Carbajal-Gomez, and G. Rodriguez-Gomez, "Generating a 50-scroll chaotic attractor at 66 MHZ by using FPGAs," *Nonlinear Dyn.*, vol. 85, no. 4, pp. 2143–2157, Sep. 2016.

[16] M. E. Yalcin, S. Ozoguz, J. A. K. Suykens, and J. Vandewalle, "N-scroll chaos generators: A simple circuit model," *Electron. Lett.*, vol. 37, no. 3, pp. 147–148, Feb. 2001.

[17] M. E. Yalcin, J. A. K. Suykens, and J. Vandewalle, "On the realization of n-scroll attractors," in *Proc. IEEE Int. Symp. Circuits Syst. (ISCAS)*, vol. 5, May/Jun. 1999, pp. 483–486.

[18] J. Q. Lu and J. D. Cao, "Adaptive complete synchronization of two identical or different chaotic (hyperchaotic) systems with fully unknown parameters," *Chaos*, vol. 15, no. 4, Nov. 2005, Art. no. 043901.

[19] J. P. Ma, L. D. Wang, S. K. Duan, and J. N. Wu, "Design of a tensile-type 3-D multi-scroll chaotic system and its application in secure communication," *J. Commun*, vol. 37, no. 12, pp. 142–155, Dec. 2016.

[20] X. R. Zhang, C. M. Wu, and W. X. Li, "Spread spectrum code construction method based on multi-vortex-chua chaos and self-coding," *Syst. Eng. Electron. Technol.*, vol. 37, no. 04, pp. 936–941, 2015.

[21] H. Li, Z. Yang, D. Yang, X. Gao, and J. Lu, "Suppressing electromagnetic interference of power converters based on 2×2-scroll chaotic PWM method," in *Proc. IEEE Int. Magn. Conf. (INTERMAG)*, Beijing, China, May 2015, p. 1.

[22] Y. H. Ding, "Research and application of high frequency isolated quasi Z source inverter," M.S. thesis, Nanjing Univ. Sci. Technol., Harrisburg, PA, USA, 2013.

[23] Z. G. Fan, H. Fan, and S. H. Xu, "Topology and SVPWM modulation strategy of the improved bi-directional Z-source converter for energy storage," *Electr. Power Autom. Equip.*, vol. 41, no. 10, pp. 3240–3248, 2015.

[24] Q. M. Cheng, Q. Zhang, Y. M. Cheng, S. Huang, and S. Y. Qi, "Passive control of grid connected photovoltaic Z source inverter based on PCHD model," *High Volt. Technol.*, vol. 42, no. 9, pp. 2723–2732, 2016.

[25] X. G. Zhang, H. T. Sun, and J. L. Zhao, "Equivalent circuit in function and topology to Chuas circuit and the design methods of these circuits," *Acta Phys. Sinica*, vol. 63, no. 20, pp. 91–98, 2014.

[26] H. G. Wu, S. Y. Chen, and B. C. Bao, "Impulsive synchronization and initial value effect for a memristor-based chaotic system," *Acta Phys. Sinica*, vol. 64, no. 3, pp. 199–206, Feb. 2015.

[27] X. F. Zhang, X. J. Chen, and Q. S. Bi, "Relaxation bursting and the mechanism of four-dimensional Chuas circuit with multiple interfaces," *Acta Phys. Sinica*, vol. 62, no. 1, p. 10502, 2013.

[28] L. G. Zhu, C. W. Shen, S. P. Zhu, and Y. Xu, "Principle and realization of chaotic SPWM modulation based on double-chaotic sequence with mutual changing parameters," *Chin. Soc. Elect. Eng.*, vol. 34, no. 30, pp. 5335–5342, 2014.

WEIHAO JIANG was born in Tai'an, Shandong, China, in 1995. He received the B.S. degree in electrical engineering from the Chongqing University of Technology, Chongqing, China, in 2018, where he is currently pursuing the M.S. degree.

His current research interests include new energy generation and control technology, and power electronic device EMI suppression.

YONG ZHENG received the B.S. degree in mechanical engineering and automation from the Qingdao University of Science and Technology, Qingdao, China, in 2005, the M.S. degree in measuring and testing technologies and instruments from the Chongqing University of Technology, in 2008, and the Ph.D. degree in measuring and testing technologies and instruments from the Hefei University of technology, in 2012.

He is currently an Assistant Professor with the Engineering Research Center of Mechanical Testing Technology and Equipment, Ministry of Education, Chongqing University of Technology. He is particularly interested in electrical detection and control.

YAN CHEN received the M.S. degree in measuring and testing technologies and instruments from the Chongqing University of Technology, in 2008, and the Ph.D. degree in electrical engineering from Chongqing University, in 2012.

She is currently an Associate Professor with the School of Electrical and Electronic Engineering, Chongqing University of Technology. From March 2015 to September 2015, she was with the Korea Advanced Institute of Science and Technology as a Visiting Scholar. She has published over 30 journal and conference papers, such as the IEEE TRANSACTIONS ON POWER ELECTRONICS and *Journal Control Theory and Applications*. Her research interests include power electronic devices, and systems and nonlinear control technology.

GUODONGXU HE was born in Chongqing, China, in 1991. He received the B.S. degree in measuring and testing technologies and instruments from the Shanghai University of Electric Power, Shanghai, China, in 2014, and the M.S. degree in electrical test and measurement technology and equipment from the Chongqing University of Technology, Chongqing, in 2019.

His current research interests include new energy generation and control technology, and power electronic device EMI suppression.

● ● ●